THE JOURNAL OF PHYSICAL CHEMISTRY B
A JOURNAL OF THE AMERICAN CHEMICAL SOCIETY

pubs.acs.org/JPCB

Article

Infrared Spectra and Hydrogen-Bond Configurations of Water Molecules at the Interface of Water-Insoluble Polymers under Humidified Conditions

Yuka Ikemoto,* Yoshihisa Harada, Masaru Tanaka, Shin-nosuke Nishimura, Daiki Murakami, Naoya Kurahashi, Taro Moriwaki, Kosuke Yamazoe, Hitoshi Washizu, Yoshiki Ishii, and Hajime Torii*

Cite This: J. Phys. Chem. B 2022, 126, 4143−4151

Read Online

ACCESS | Metrics & More | Article Recommendations | Supporting Information

ABSTRACT: Elucidating the state of interfacial water, especially the hydrogen-bond configurations, is considered to be key for a better understanding of the functions of polymers that are exhibited in the presence of water. Here, an analysis in this direction is conducted for two water-insoluble biocompatible polymers, poly(2-methoxyethyl acrylate) and cyclic(poly(2-methoxyethyl acrylate)), and a non-biocompatible polymer, poly(*n*-butyl acrylate), by measuring their IR spectra under humidified conditions and by carrying out theoretical calculations on model complex systems. It is found that the OH stretching bands of water are decomposed into four components, and while the higher-frequency components (with peaks at ∼3610 and ∼3540 cm^{-1}) behave in parallel with the C═O and C−O−C stretching and CH deformation bands of the polymers, the lower-frequency components (with peaks at ∼3430 and ∼3260 cm^{-1}) become pronounced to a greater extent with increasing humidity. From the theoretical calculations, it is shown that the OH stretching frequency that is distributed from ∼3650 to ∼3200 cm^{-1} is correlated to the hydrogen-bond configurations and is mainly controlled by the electric field that is sensed by the vibrating H atom. By combining these observed and calculated results, the configurations of water at the interface of the polymers are discussed.

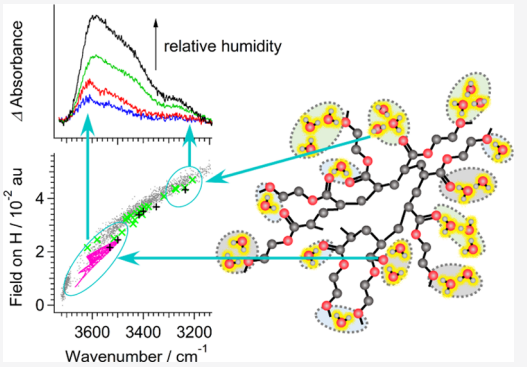

1. INTRODUCTION

Polymers often exhibit their functions in water, or in the presence of water, that is not just a solvent but plays an important role in the expression of functions. The water molecules related to those functions exist in the vicinity of the polymers and, compared to bulk water, have different properties, which have been studied by various techniques such as differential scanning calorimetry (DSC),[1,2] neutron reflectometry,[3−5] atomic force microscopy,[6] and contact angle measurements.[7,8] Vibrational spectroscopy has been used to analyze the structural and dynamical properties of aqueous solutions.[9−14] The state of water in various polymers has often been studied by analyzing the OH stretching bands obtained from IR spectroscopy,[15−19] with the expectation that abundant information with regard to the nature of hydrogen bonding is contained in the band shapes. However, the mechanisms that determine the band shapes seem complicated, so that the discussions on the state of water in polymers are often limited to a qualitative level.

The system examined in the present study is the interface of water-insoluble biocompatible and non-biocompatible polymers. Water-insoluble biocompatible polymers have an inhibitory effect on the adsorption of proteins and are widely used as coating materials for medical devices. Regarding the mechanism of biocompatibility, Tanaka et al. proposed, from DSC measurements, a model in which the water molecules at or around the interface of the polymers are classified into non-freezing water (located closest to the interface), intermediate water, and free water (located farthest from the interface), and among these, intermediate water plays a key role in biocompatibility.[20,21] In addition, time-resolved ATR-IR spectra were measured during the water adsorption process, and the frequency positions of the observed OH stretching bands were discussed in relation to the classification of water.[22,23]

The aim of the present study is to clarify the state of water at the interface of those polymers more quantitatively by combining IR spectroscopy and theoretical calculations. To measure the IR spectra in a static state without interference of free water, measurements under humidified conditions were performed. In this way, it is expected that the behavior of interfacial water is most clearly seen. Theoretical calculations

Received: March 10, 2022
Revised: May 12, 2022
Published: May 31, 2022

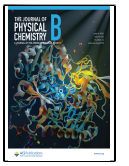

https://doi.org/10.1021/acs.jpcb.2c01702
J. Phys. Chem. B 2022, 126, 4143−4151

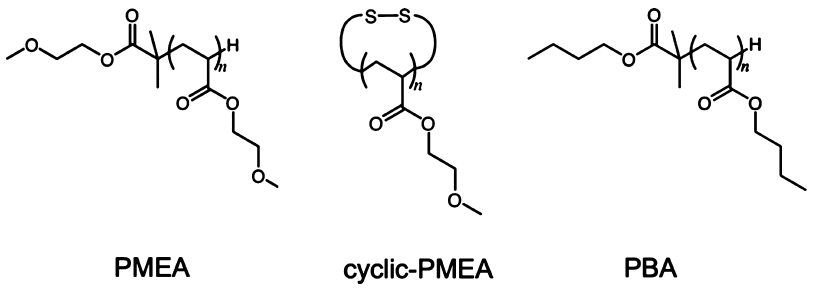

Figure 1. Chemical structures of PMEA, cyclic-PMEA, and PBA.

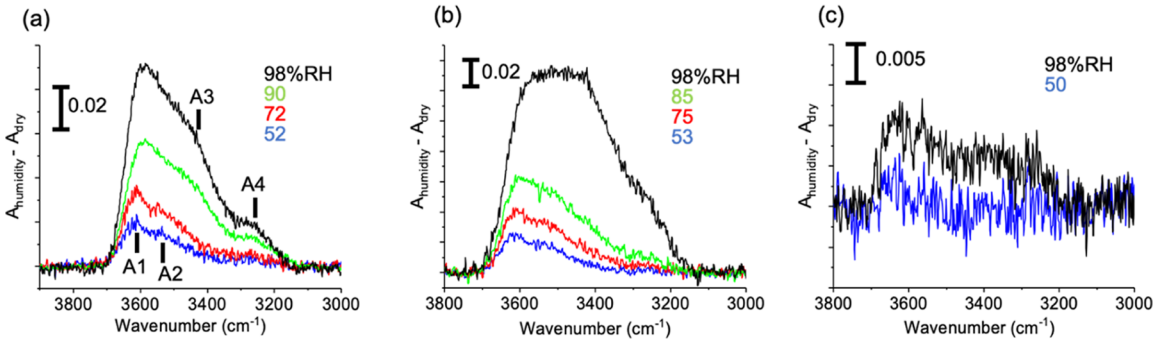

Figure 2. Difference absorption spectra of (a) PMEA, (b) cyclic-PMEA, and (c) PBA in the wavenumber region of the OH stretching mode. The dry spectrum was subtracted from the humidified spectrum whose relative humidity is indicated beside the peak. The absorbance scale is indicated by the bar. The OH bands have four components at 3610, 3540, 3430, and 3260 cm^{-1}, which are labeled as A1 to A4 in (a).

were carried out on a number of complexes consisting of water molecules and model compounds representing the hydrogen-bond-accepting functional groups in the polymers to support the discussion on the effects of humidity on the vibrational spectra. The factors that determine the frequency positions of the OH stretching bands are discussed at a quantitative level, on the basis of which the meaning of the observed IR spectra in relation to the hydrogen-bond configurations at the polymer−water interface is discussed.

2. EXPERIMENTAL AND COMPUTATIONAL PROCEDURES

Polymers examined in the present study are poly(2-methoxyethyl acrylate) (PMEA),[20,24] cyclic(poly(2-methoxyethyl acrylate)) (cyclic-PMEA),[25] and poly(*n*-butyl acrylate) (PBA).[20,24] The chemical structures, properties, and synthesis methods of these polymers are described in Figure 1.

IR spectra (in the mid-IR region from 600 to 8000 cm^{-1}) were measured on the IR beamline BL43IR at the SPring-8 synchrotron facility. The wavenumber resolution was 2 cm^{-1} and accumulated number was 100. The humidity dependence of absorption spectra was measured using a humidity controlling cell, which is illustrated in Figure S1 in the Supporting Information. Each polymer was cast on a silicon wafer for IR measurements. To calibrate the polymer thickness, the observed absorption spectra were normalized by the integrated intensity of the C=O stretching band. The amount of water adsorbed into the polymers at humidified conditions was estimated by the OH stretching band. Detailed descriptions of the experimental procedures and sample preparation are provided in the Supporting Information.

To support the discussion on the effects of humidity on the vibrational spectra, calculations were carried out for the following types of complexes related to acetone (a model of the carbonyl groups in a polymer) and/or dimethyl ether (a model of the C−O−C groups in a polymer) interacting with water: (1) complexes of either acetone or dimethyl ether with 1−3 water molecules with full geometry optimization to cover a variety of possible hydrogen-bond configurations, including a bifurcated configuration (with a water oxygen atom that accepts two hydrogen bonds from other water molecules) and a (topologically) linear hydrogen-bond chain of water, (2) complexes of either acetone or dimethyl ether with a water molecule with specified angular hydrogen-bond configurations [defined by the inclination θ and azimuth φ of the spherical polar coordinate system around the carbonyl or ether O atom], (3) complexes of either acetone or dimethyl ether buried in a cavity made around the center of the $(water)_{90}$ clusters with full geometry optimization, and (4) complexes consisting of two molecules of acetone and/or dimethyl ether with one water molecule in the bridging hydrogen-bond configurations. Hereafter, we denote these types of complexes as 1a, 2e, and so forth, where characters a and e stand for acetone and ether, respectively. Taking into account that the ether group in the side chain of PMEA is separated from the ester group by two methylene (CH_2) groups, the inductive effect discussed in a previous study[26] is not considered to be relevant in the present case. Details of the structural characteristics of these complexes are given in the Supporting Information.

The vibrational properties were examined for the normal isotopic species of all these complexes, as well as for isotopically diluted complexes with all but one hydrogen atom of water (interacting directly with acetone or dimethyl ether) being deuterated to remove the effects of vibrational couplings among the OH stretches. The electric field operating on the vibrating H atom along each OH bond was also calculated. All the abovementioned calculations were carried out at the B3LYP/6-31+G(2df,p) level of density functional theory by using the Gaussian 09 program.[27] The calculated

https://doi.org/10.1021/acs.jpcb.2c01702
J. Phys. Chem. B 2022, 126, 4143−4151

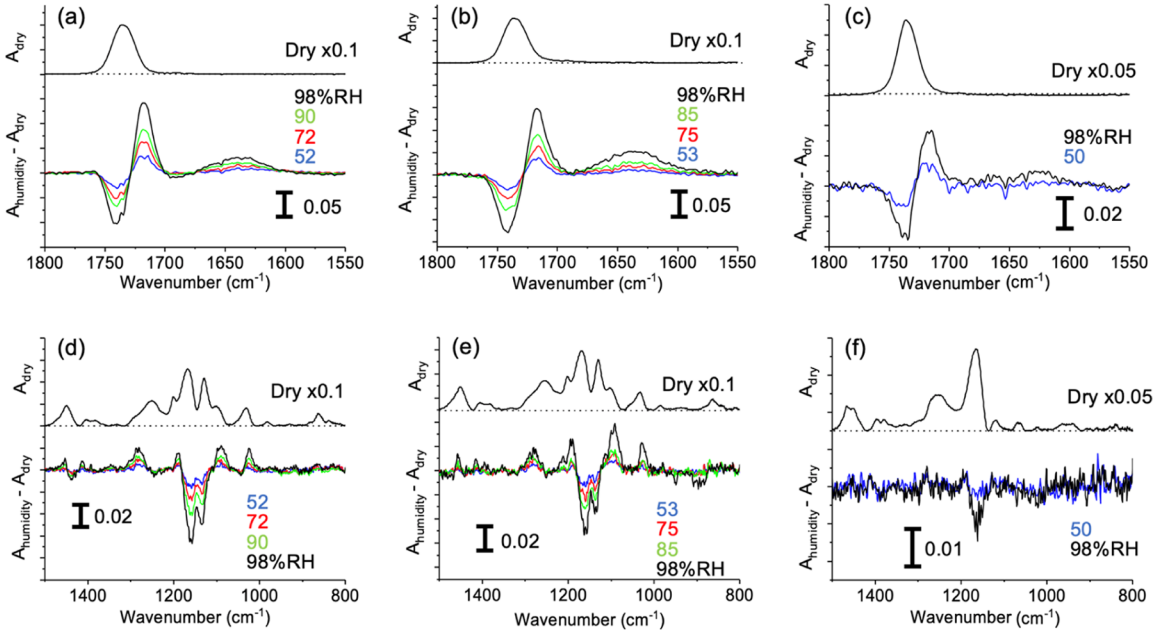

Figure 3. Difference absorption spectra of (a,d) PMEA, (b,e) cyclic-PMEA, and (c,f) PBA in the wavenumber region of (a−c) C═O stretching mode and (d−f) C−O−C stretching and CH deformation modes. The dry spectrum was subtracted from the humidified spectrum whose relative humidity is indicated beside the peak. The absorbance scale is indicated by the bar. The dry spectrum is shown at the top. The intensity of the dry spectrum was multiplied by 0.1 in (a,b,d,e) and 0.05 in (c,f).

vibrational frequencies were scaled by a factor of 0.95935, which was determined[28] by referring to the observed[29] and calculated frequencies of an isolated HDO molecule in the gas phase.

3. RESULTS AND DISCUSSION

3.1. Results of IR Spectroscopy under Humidified Conditions. Figure 2a−c shows the difference absorption spectra of PMEA, cyclic-PMEA, and PBA, respectively, in the wavenumber region of the OH stretching mode. The spectrum measured under dry conditions (shown in Figure S2 in the Supporting Information) was subtracted from that observed at each RH indicated beside the peak. The absorbance scale is indicated by the bar. The OH stretching band observed in Figure 2 is due to the water molecules adsorbed into the polymers. The band intensity increases with increasing RH. In Figure 2a, we can recognize four components that are labeled as A1 to A4. At a RH of 52%, the spectrum consists of A1 and A2 components located at about 3610 and 3540 cm^{-1}, respectively. Upon increasing RH to 72%, the A3 component appears at 3430 cm^{-1}, and at the highest RH of 98%, the A4 component appears at 3260 cm^{-1}. The spectral change with humidification observed for cyclic-PMEA is similar, as shown in Figure 2b, but the intensity grows faster and the A3 and A4 components are much higher at the highest RH than in the spectra of PMEA. On the other hand, the OH stretching band observed for PBA is weak even at the highest RH but has a tail to a lower wavenumber region extending to ∼3250 cm^{-1}, as shown in Figure 2c. The weak intensity means that only few water molecules are adsorbed into PBA by humidification. The OH stretching band intensity at the highest RH reflects the saturated water content of each polymer. The average number of adsorbed water molecules per monomer was estimated from the total integrated intensity of the OH stretching band in the IR absorption spectrum of each polymer with saturated water content, in a way described in detail in the Supporting Information. The estimated numbers are 0.27, 0.44, and 0.01 for PMEA, cyclic-PMEA, and PBA, respectively, at the highest RH.

Figure 3 (a,d), (b,e), and (c,f) show the difference spectra of PMEA, cyclic-PMEA, and PBA, respectively, in the wavenumber regions of (a−c) the C═O stretching mode and (d−f) the C−O−C stretching and CH deformation modes. The RH of each spectrum is indicated in the figure, and the dry spectrum of each polymer is shown at the top. In the C═O stretching mode region shown in Figure 3a−c, the difference spectra have negative and positive features centered at 1740 and 1718 cm^{-1}, so that the frequency shift is estimated to be 22 cm^{-1}. The widths of these features are 24 cm^{-1}. This low wavenumber shift is considered to arise from hydrogen bonding. With increasing RH, the amplitudes of these negative and positive features increase without changing the center wavenumbers. It implies that the number of the hydrogen-bonded C═O sites increases with humidification. These spectral changes are common in shape among the three polymers, but the amplitudes are obviously small for PBA. This is consistent with the small intensity of the OH stretching band shown in Figure 2c, which indicates that the amount of adsorbed water is low. In Figure 3a−c, the OH deformation band is also observed at 1635 cm^{-1}, with its intensity increasing with humidification. In the wavenumber region shown in Figure 3d,e, we can recognize two negative features located at 1160 and 1136 cm^{-1}, which are considered to be related to the C−O−C stretching modes of the ester and ether groups. There are also positive features related to the CH deformation modes. The intensities of these features are enhanced with increasing RH, but no wavenumber shift is observed. The spectra in (f) have only a small structure related to ester C−O−C.

The integrated areas of the component bands observed in the OH stretching region (shown in Figure 2) of the spectra of PMEA, cyclic-PMEA, and PBA are plotted versus RH in Figure

https://doi.org/10.1021/acs.jpcb.2c01702
J. Phys. Chem. B 2022, 126, 4143−4151

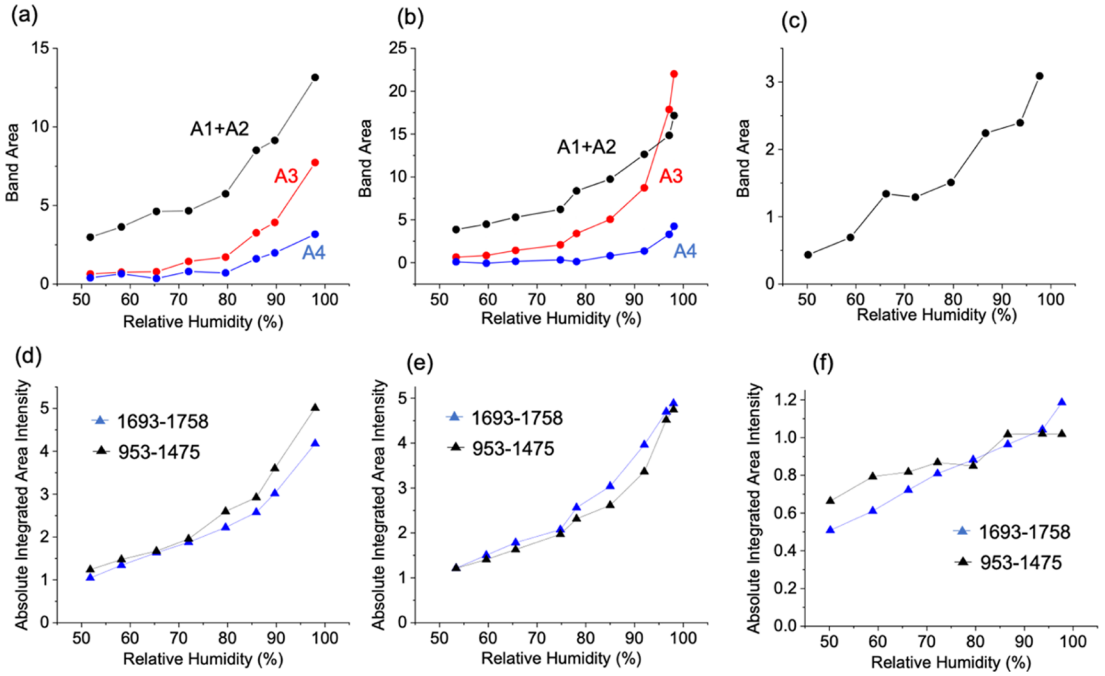

Figure 4. Analysis of humidity dependence of (a,d) PMEA, (b,e) cyclic-PMEA, and (c,f) PBA. (a,b) Integrated areas of the A1 + A2 (black dots), A3 (red dots), and A4 (blue dots) components in the OH stretching region (shown in Figure 2). (c) Integrated area of whole OH bands of the spectrum of PBA. (e–f) Integrated intensities of the difference spectra in the wavenumber regions from 1693 to 1758 cm^{-1} (the C═O stretching band region shown in Figure 3a–c, blue triangles) and from 953 to 1475 cm^{-1} (the C–H deformation and C–O–C stretching band region shown in Figure 3d–f, black triangles).

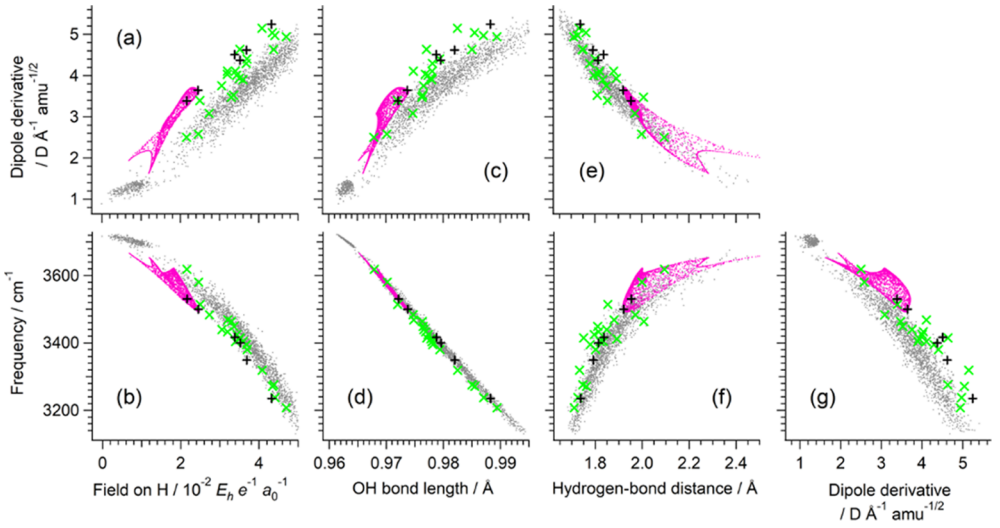

Figure 5. Plots of the (a,c,e) dipole derivative and (b,d,f,g) vibrational frequency (scaled) of the OH stretching mode against the (a,b) electric field on the vibrating hydrogen atom (the component along the OH bond), (c,d) OH bond length, (e,f) hydrogen-bond distance, and (g) dipole derivative of the OH stretching mode calculated for the acetone + $n$$H_2O$ complexes (n = 1–3, with full geometry optimization, black +), the acetone + H_2O complexes with variously fixed angular hydrogen-bond configurations (pink dots), and the complexes of acetone buried in a cavity made around the center of the $(water)_{90}$ clusters with full geometry optimization (green ×), overlapped on the results obtained[28] for the OH stretches of the $(water)_{90}$ clusters (gray dots). With regard to the complexes involving acetone, the stretching of the OH bond directly interacting with acetone is considered, and [including the case of the $(water)_{90}$ clusters] the hydrogen atoms other than the vibrating one are deuterated.

4a–c, respectively. Here, the spectra measured at some RH values not explicitly shown in Figure 2 are also included in this analysis. For PMEA and cyclic-PMEA, both components A1 and A2 are observed together from RH ∼ 50%, as shown in Figure 2, and so, the sums of their band areas are plotted with black circles in Figure 4a,b. The red and blue circles show the areas of A3 and A4 components, respectively. For PBA shown in (c), the integrated intensity of the whole OH stretching band is plotted because the intensity is too low for reliable deconvolution. We can recognize in Figure 4a,b that the intensity of A1 + A2 gradually increases between RH 50 and 70% and more steeply in the higher RH region. The intensity of A3 starts increasing at higher RH and that of A4 starts increasing at even higher RH. The increase of A3 in cyclic-PMEA is steeper, and the intensity at the highest RH is larger than in PMEA. In contrast, with regard to PBA shown in

https://doi.org/10.1021/acs.jpcb.2c01702
J. Phys. Chem. B 2022, 126, 4143–4151

Figure 4c, the intensity remains low and increases only slightly with RH. Figure 4d–f shows the integrated intensities of the difference spectra in the wavenumber regions from 1693 to 1758 cm^{-1} (the C═O stretching band region shown in Figure 3a–c, blue triangles) and from 953 to 1475 cm^{-1} (the CH deformation and C–O–C stretching band region shown in Figure 3d–f, black triangles) plotted versus RH. It is recognized that the curves in (d,e) are similar to those of A1 + A2 in (a,b). The curve in (f) is also similar to that in (c), but the value is very small. These results indicate that both the carbonyl and ether groups play an important role in water adsorption. The rapid increases with RH that are seen for the components A3 and A4 in (a,b) do not have any counterparts in (d,e) [even if we take into account the IR intensity enhancement upon hydrogen-bond formation due to the non-Condon effect[30,31] discussed in Section 3.2]. This suggests that there exist some excess water molecules that are not directly hydrogen-bonded to either the carbonyl or ether group in the polymer.

3.2. Results of Theoretical Calculations. The vibrational frequency and the dipole derivative (of isotopically diluted species) plotted against the electric field operating on the H atom, the OH bond length, and the hydrogen-bond distance, as well as the correlation between these two vibrational properties, calculated for the complexes of types 1a, 2a, and 3a are shown in black and color dots and markers in Figure 5, overlapped on the plots of the results obtained[28] for the OH stretches of the isotopically diluted $(water)_{90}$ clusters shown with gray dots. It is clearly seen in panel d of this figure that the frequency (including type 2a shown with pink dots) is linearly correlated with the OH bond length, supporting the idea that constraints on softer modes (C═O···H bending and C–C═O···H torsion) do not essentially have any harmful effect on the properties of harder modes (OH stretches). It is also seen that reasonably good correlations are obtained among the structural, vibrational, and electrostatic properties as shown in the other six panels of Figure 5. According to the mechanism discussed in ref 28, the frequency is shifted mainly by the interaction between the dipole derivative and the electric field. Since the dipole derivative is enhanced by the electric field (known as the non-Condon effect[30,31]), as shown in Figure 5a, the frequency is nonlinearly dependent on the electric field, as shown in Figure 5b. [As a result, the infrared intensity per OH bond is larger for a lower-frequency mode, as shown in Figure 5g]. The same set of plots obtained for the complexes of types 1e, 2e, and 3e is shown in Figure S5 in the Supporting Information. By using the results obtained[28] for the OH stretches of the $(water)_{90}$ clusters shown with gray dots as a reference, it is recognized that the correlations do not largely depend on the functional group of the hydrogen-bond acceptor (>C═O or C–O–C). It is also clear that the stretching frequencies of the dangling OH groups are as high as ~3700 cm^{-1} because the electric fields sensed by all those OH bonds are small.

The abovementioned result indicates that the frequency calculated for the complexes of type 2a (acetone···water 1:1 complexes) is distributed in a rather wide range of about 3500–3650 cm^{-1}. This is because the frequency depends on the θ and φ angles. The frequency (of HDO) is calculated as 3622 cm^{-1} at θ = 0° (linear C═O···H configuration) and shifts to the low-frequency side as θ increases to ~60°. The extent of the frequency shift is the largest at φ = 0° (down to 3492 cm^{-1}), where the H atom of water is located on the plane of the carbonyl group, and is the smallest at φ = 90° (down only to 3609 cm^{-1}), where the H atom of water is located out of the plane. A similar dependence is also recognized for the lower-frequency OH stretch (corresponding to the OH symmetric stretch of an isolated water molecule) of the normal isotopic species. The behavior of these frequency shifts is described in more detail in the Supporting Information.

From the plots for the complexes of types 1a and 3a shown in Figure 5, it is recognized that the frequencies of some of those complexes are significantly lower than those of the 1:1 complexes (type 2a), with the frequency range extending to ~3200 cm^{-1}. Some insights would be obtained by examining the results for the complexes of type 1a, which are summarized in Figure 6. Here, each hydrogen-bonded OH (supposed as belonging to molecule D and donating a hydrogen bond to molecule A) is characterized by the M value defined, by modifying from that in ref 32, as $M = -d' + a' + d'' - a'' + \delta$, where d' and a' are the number of hydrogen bonds donated and accepted by molecule D, d'' and a'' are the number of hydrogen bonds donated and accepted by molecule A (without counting the hydrogen bond between D and A), and δ is 1 if A is a carbonyl or ether O atom and 0 otherwise. The frequency (of the lower-frequency OH stretch of the normal isotopic species) is calculated as 3487 cm^{-1} for the optimized structure of the 1:1 complex [with (θ, φ) = (60.7, 1.7°)] and also as ~3500 cm^{-1} (3509 and 3523 cm^{-1}) for the 1:2 complex if both of the water molecules are hydrogen-bonded directly to C═O. However, when the water molecule that is hydrogen-bonded to C═O receives a hydrogen bond from another water molecule, the OH stretching frequency (delocalized over the two hydrogen-bonded OH bonds) shifts down to ~3400

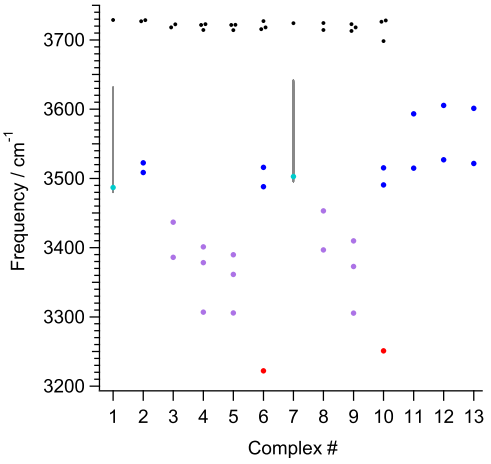

Figure 6. Vibrational frequencies (scaled) calculated for the normal isotopic species of the complexes of types 1a and 1e (numbered as 1–10 for the structures shown in part a–j of Figure S3 in the Supporting Information) and type 4 (numbered as 11–13 for the structures shown in part a–c of Figure S4 in the Supporting Information). For the modes that are sufficiently isolated and for those delocalized over the bonds of the same M value, the nature of the OH bond that mainly contributes to each mode is indicated by the M value as M = 0 (blue), 1 (light blue), and 3 (red). The modes that are delocalized over the bonds of M = 1 and 2 are shown with purple markers. The stretching modes of dangling OH bonds are shown with black markers. For some complexes, the markers are displaced horizontally to clearly show two or more closely located data. The frequency range obtained for the complexes of type 2a or 2e is also shown with a gray bar overlapped with the markers for complexes 1 and 7, respectively.

https://doi.org/10.1021/acs.jpcb.2c01702
J. Phys. Chem. B 2022, 126, 4143–4151

cm^{-1} (3386 and 3437 cm^{-1}) [The decoupled OH stretch of HDO also shifts to this frequency region, as shown in Figure S9 in the Supporting Information]. The frequency region of these delocalized OH stretching modes extends further to ~3300 cm^{-1} when a (topologically) linear hydrogen-bond chain of water is formed, and when the O atom of the innermost OH receives hydrogen bonds from two water molecules in a bifurcated hydrogen-bond configuration (M = 3), the stretching frequency of this innermost OH shifts further down to 3222 cm^{-1}. As shown in Figure 5b, all these frequencies are controlled mainly by the electric field operating on the vibrating H atom. Similar results are obtained for the complexes of type 1e and 3e, as also summarized in Figure 6.

In the case of the bridging hydrogen-bond configuration (type 4), the two OH stretching modes of the normal isotopic species are characterized as the symmetric and antisymmetric stretches because both OH bonds are hydrogen-bonded with similar strength. It is shown in Figure 6 that the frequencies of those modes are calculated as 3515 and 3593 cm^{-1} when a water molecule is bridging to two C═O groups of acetone molecules. Similar results are obtained for the cases where one or both of the hydrogen-bond accepting groups are replaced by C−O−C.

All these results suggest that we can detect the hydrogen-bonding conditions of the water molecules adsorbed on the hydrogen-bond-accepting functional groups in a polymer by analyzing the vibrational spectral features.

3.3. Discussions on Water Structures Adsorbed at the Interface of the Polymers. Based on the results of the experiments and the calculations, we will discuss the state of water molecules adsorbed at the interface of the polymers under a humidified environment.

As shown in Figure 6 (as well as in Figure S6 in the Supporting Information), when a water molecule is hydrogen-bonded to a carbonyl group or an ether group (or more generally, any group with the C−O−C structure) without accepting any hydrogen bond from another water molecule ($M \leq 1$, shown with blue and light blue markers in Figure 6), the lower bound of the OH stretching frequency is estimated as ~3480 cm^{-1}. In other words, according to Figure 5b (as well as Figure S5b in the Supporting Information), this indicates the upper bound of the magnitude of the electric field that is sensed by donating only a single hydrogen bond without accepting any hydrogen bond. Therefore, OH stretching bands observed at lower wavenumbers are considered to arise from water molecules that accept one or more hydrogen bonds or from clusters involving such water molecules. The A3 and A4 components (located at 3430 and 3260 cm^{-1}) observed at middle to high RH in Figure 2a,b correspond to this. Indeed, as shown in Figure 4, the rapid increase of intensity with RH is recognized for the A3 and A4 components of the OH stretching bands (panels a and b of the figure) but not for the bands of the polymers (panel d and e), supporting the existence of water molecules that are not directly hydrogen-bonded to either the carbonyl or ether group. More specifically, as indicated in Figure 6, when a water molecule donating a hydrogen bond to a carbonyl or ether group accepts only one hydrogen bond, forming a linear hydrogen-bond chain, the lower bound of the OH stretching frequency is estimated as ~3300 cm^{-1}. At high RH ≥ 85%, the A4 component appears at a lower wavenumber, as shown in Figures 2 and 4, indicating that small water clusters with bifurcated (typically M = 3, shown with red markers in Figure 6) hydrogen-bond configurations are formed at the interface of the polymers. Especially the rather small but rapid increase of the intensity of this component observed for cyclic-PMEA should be noted. This may be regarded as an early stage of the formation of intermediate water that is considered to play a key role in biocompatibility of the polymers.[20,21] In the case of PBA, there are only few adsorbed water molecules because the OH stretching band shown in Figure 2c is very weak. However, since the spectrum has a tail to a lower wavenumber region extending to ~3250 cm^{-1}, it is considered that the water molecules adsorbed into this polymer form some clusters. According to Figure 5b (as well as Figure S5b in the Supporting Information), all these vibrational frequencies are controlled mainly by the electric field sensed by each vibrating OH bond.

Various hydrogen-bond configurations that are considered to be formed at the interface of the polymers are schematically illustrated in Figure 7. The structures with a bifurcated hydrogen bond are represented as d-trimer(bif) and s-trimer(bif), while the structures with a linear hydrogen-bond chain are represented as dimers [d-dimer(lin) and s-dimer(lin)] and linear trimers [d-trimer(lin) and s-trimer(lin)]. Here, d- and s- indicate whether the hydrogen-bond accepting group of the polymer is carbonyl (involved in C═O *d*ouble bond) or ether (or ester, involved in C−O−C *s*ingle bond). The A3 and A4 components of the OH stretching band are considered to arise from these configurations. As shown in Figure 3, both of these functional groups of the polymers are involved as hydrogen bond acceptors of water at the interface. The distribution of various hydrogen-bond configurations shown in Figure 7 is reflected in the observed band widths of these functional groups.

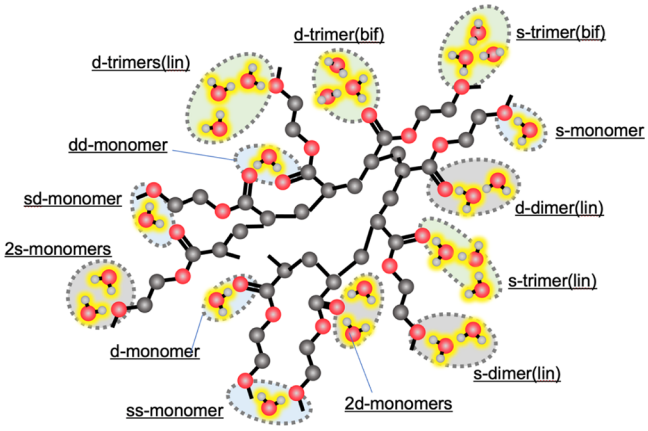

Figure 7. Illustration of various possible hydrogen-bond configurations at the interface of the polymers. The structures represented as d-trimer(bif) and s-trimer(bif) have a bifurcated hydrogen bond, while the structures represented as dimers [d-dimer(lin) and s-dimer(lin)] and linear trimers [d-trimer(lin) and s-trimer(lin)] have a linear hydrogen-bond chain. The characters d- and s- indicate whether the hydrogen-bond-accepting group of the polymer is carbonyl (involved in C═O *d*ouble bond) or ether (or ester, involved in C−O−C *s*ingle bond).

Then, what kind of configurations may be considered for the A1 and A2 components of the OH stretching band that are present even at low RH? Taking into account the discussion made above, in which small water clusters at the interface of the polymers are considered at high humidity, it would be most

https://doi.org/10.1021/acs.jpcb.2c01702
J. Phys. Chem. B 2022, 126, 4143−4151

reasonable to suppose that the configurations with a single water molecule hydrogen-bonded to the polymer are formed at sufficiently low humidity. The correlation between the spectral intensity changes of the OH stretching band and the polymer bands shown in Figure 4, and the frequency ranges of various hydrogen-bond configurations shown in Figure 6 would support this idea. As clearly recognized from the spectral changes shown in Figure 4, both the carbonyl and ether groups are considered to be involved in such configurations. These configurations are labeled as d-monomer and s-monomer in Figure 7. The vibrational frequencies would not change much even if two water molecules are hydrogen-bonded separately to one hydrogen-bond acceptor (2d-monomer and 2s-monomer in Figure 7). At a higher humidity, the A1 and A2 components may also arise from the water molecules at the peripherals of clusters, such as those shown with blue markers (M = 0) for complexes 6 and 10 in Figure 6.

With regard to the frequency distributions of the A1 and A2 components, the following three possibilities may be considered. One is the angular distributions of the hydrogen bond. As shown in Figure 6 (as well as in Figure S6 in the Supporting Information), the OH stretching frequency depends strongly on the angular configuration of the hydrogen bond, ranging from ∼3500 to ∼3600 cm^{-1}. For example, if the hydrogen bond on the C═O group is made rather linear (i.e., $\theta \cong 0°$) or out of the carbonyl plane (i.e., $\varphi \cong 90°$) due to some steric reasons of the polymer, the OH stretching frequency would be ∼3600 cm^{-1} rather than ∼3500 cm^{-1}. Another possibility is the formation of the bridging configurations, in which a water molecule straddles two hydrogen-bond acceptor groups of the polymer. As shown in Figure 6, for all the three complexes of type 4 (complexes 11−13), the symmetric and antisymmetric OH stretches are calculated at ∼3520 cm^{-1} (in the range of 3515−3526 cm^{-1}) and at ∼3600 cm^{-1} (in the range of 3593−3605 cm^{-1}), respectively. In other words, not only the carbonyl group (as reported in ref 23) but also the ether group may be involved in such configurations. The frequency splitting between the two modes is totally of intramolecular origin because the two modes are essentially degenerate for HDO, as shown in Figure S9 in the Supporting Information. These configurations are labeled as dd-monomer, ss-monomer, and sd-monomer in Figure 7. Yet another possibility would be the distribution of the hydrogen-bond distance. As shown in Figure 5 (as well as in Figures S5 and S6 in the Supporting Information), the OH stretching frequency is well correlated to the hydrogen-bond distance. A rather long hydrogen bond (longer than 2.2 or 2.3 Å) corresponds to the OH stretching frequency of >3600 cm^{-1}, while a shorter hydrogen bond gives rise to a shift to a lower frequency. As a result, when the hydrogen-bond distance fluctuates dynamically because of thermal motions or is distributed statically for steric or some other reasons, frequency distributions of the OH stretching band would be generated. In fact, the existence of completely dangling OH bonds of water is not realistic around polymers, and there is no IR band observed at ∼3700 cm^{-1} (corresponding to the frequencies of the gas-phase water molecule) in the spectra shown in Figure 2, even if we take into account the intrinsically weak IR intensity of those bands.

Recently, some of the present authors have found that it is possible to distinguish the characteristics of water molecules inside the condensed organic−water complex by employing molecular dynamics (MD) simulations.[33] Therefore, to quantitatively evaluate the relative contributions of the abovementioned three possibilities, information derived from MD simulations is considered to be most helpful. Theoretical analyses on this point will be deferred to later studies.

4. CONCLUDING REMARKS

In the present study, by combining IR spectroscopy under humidified conditions (RH from 50 to 98%) and theoretical calculations on model complex systems, we have examined the state of water at the interface of two water-insoluble biocompatible polymers, PMEA and cyclic-PMEA, and a non-biocompatible polymer PBA, with a focus on hydrogen-bond configurations. The following four points are considered to be especially noteworthy. (1) The OH stretching band consists of four components, labeled as A1 (3610 cm^{-1}), A2 (3540 cm^{-1}), A3 (3430 cm^{-1}), and A4 (3260 cm^{-1}). As shown in Figure 4, the A1 and A2 components are present even at a low RH of ∼50% and are enhanced upon increasing RH in parallel with the carbonyl- and ether-related bands of the polymers, while the lower-frequency A3 and A4 components appear at a higher RH and are enhanced more steeply upon increasing RH. The intensity and the extent of enhancement depend on the specific polymer species. (2) Changes in the intensity and/or shape are recognized for both the carbonyl- and ether-related bands upon increasing RH, as shown in Figure 3, indicating that both of these groups are involved in the hydrogen bonding with interfacial water. (3) The results of the theoretical calculations show that the OH stretching frequency, which is distributed from ∼3650 to ∼3200 cm^{-1}, is mainly controlled by the electric field sensed by the vibrating H atom, as shown in Figure 5b, and, hence, is correlated to the hydrogen-bond configurations, that is, the number of donating and accepting hydrogen bonds that may be roughly summarized as the M value defined in Section 3.2, as well as the distance and angular properties of each hydrogen bond. (4) Based on the results of these experiments and calculations, the A3 and A4 components of the OH stretching band that are observed at lower wavenumbers are considered to arise from water molecules that accept one or more hydrogen bonds or from clusters involving such water molecules, which are shown as dimers and trimers in Figure 6. With regard to the A1 and A2 components, three possibilities are suggested, that is, the angular distributions of the hydrogen bond, the symmetric and antisymmetric OH stretches of water bridging to the carbonyl and/or ether groups of the polymer, and the distribution of the hydrogen-bond distance.

All the abovementioned results clearly indicate that IR measurements under humidified conditions, combined with theoretical analysis, are useful for elucidating the state of water at the interface of polymers. The information obtained in the present study will constitute the basis for further examination of the state of interfacial water, for example, with regard to the relation between detailed spatial characteristics and vibrational frequency distributions, which will be dealt with in future studies.

■ ASSOCIATED CONTENT

Supporting Information

The Supporting Information is available free of charge at https://pubs.acs.org/doi/10.1021/acs.jpcb.2c01702.

Details of the experimental and computational procedures and experimental and calculated results (PDF)

https://doi.org/10.1021/acs.jpcb.2c01702
J. Phys. Chem. B 2022, 126, 4143−4151

AUTHOR INFORMATION

Corresponding Authors

Yuka Ikemoto − *Spectroscopy Division, Japan Synchrotron Radiation Research Institute, Sayo, Hyogo 679-5198, Japan;* orcid.org/0000-0001-6266-0977; Email: ikemoto@spring8.or.jp

Hajime Torii − *Department of Applied Chemistry and Biochemical Engineering, Faculty of Engineering, and Department of Optoelectronics and Nanostructure Science, Graduate School of Science and Technology, Shizuoka University, Hamamatsu 432-8561, Japan;* orcid.org/0000-0002-6061-9599; Email: torii.hajime@shizuoka.ac.jp

Authors

Yoshihisa Harada − *Institute for Solid State Physics, The University of Tokyo, Kashiwa, Chiba 277-8581, Japan; Synchrotron Radiation Research Organization, The University of Tokyo, Bunkyo-ku, Tokyo 113-8656, Japan;* orcid.org/0000-0002-4590-9109

Masaru Tanaka − *Institute for Material Chemistry and Engineering and Graduate School of Engineering, Kyushu University, Fukuoka 819-0395, Japan;* orcid.org/0000-0002-1115-2080

Shin-nosuke Nishimura − *Institute for Material Chemistry and Engineering, Kyushu University, Fukuoka 819-0395, Japan;* Present Address: Faculty of Science and Engineering, Department of Molecular Chemistry and Biochemistry, Doshisha University, 1-3 Tatara Miyakodani, Kyotanabe, Kyoto 610-0394, Japan; orcid.org/0000-0001-6857-5095

Daiki Murakami − *Institute for Material Chemistry and Engineering and Graduate School of Engineering, Kyushu University, Fukuoka 819-0395, Japan;* Present Address: Department of Biological and Environmental Chemistry, Faculty of Humanity-Oriented Science and Engineering, Kindai University, 11-6 Kayanomori, Iizuka, Fukuoka, 820-8555, Japan; orcid.org/0000-0002-5552-4384

Naoya Kurahashi − *Institute for Solid State Physics, The University of Tokyo, Kashiwa, Chiba 277-8581, Japan; Synchrotron Radiation Research Organization, The University of Tokyo, Bunkyo-ku, Tokyo 113-8656, Japan*

Taro Moriwaki − *Spectroscopy Division, Japan Synchrotron Radiation Research Institute, Sayo, Hyogo 679-5198, Japan*

Kosuke Yamazoe − *Institute for Solid State Physics, The University of Tokyo, Kashiwa, Chiba 277-8581, Japan; Synchrotron Radiation Research Organization, The University of Tokyo, Bunkyo-ku, Tokyo 113-8656, Japan;* Present Address: Japan Synchrotron Radiation Research Institute, 1-1-1 Kouto, Sayo, Hyogo 679-5198, Japan; orcid.org/0000-0002-7249-7090

Hitoshi Washizu − *Graduate School of Information Science, University of Hyogo, Kobe, Hyogo 650-0047, Japan;* orcid.org/0000-0002-5787-7204

Yoshiki Ishii − *Graduate School of Information Science, University of Hyogo, Kobe, Hyogo 650-0047, Japan;* orcid.org/0000-0003-0102-9326

Complete contact information is available at: https://pubs.acs.org/10.1021/acs.jpcb.2c01702

Notes

The authors declare no competing financial interest.

ACKNOWLEDGMENTS

This study was supported by JSPS KAKENHI Grant-in-Aid for Scientific Research on Innovative Areas: Aquatic Functional Materials (grant numbers JP19H05717, JP19H05718, JP19H05720, and JP20H05215). Synchrotron radiation measurements were performed at SPring-8 with the approval of the Japan Synchrotron Radiation Research Institute (2018B1243, 2019B0953, 2020A0953, 2020A1315, 2020A1756, 2020A1779, 2021A1488, and 2021B1363).

REFERENCES

(1) Ping, Z. H.; Nguyen, Q. T.; Chen, S. M.; Zhou, J. Q.; Ding, Y. D. States of Water in Different Hydrophilic Polymers − DSC and FTIR Studies. *Polymer* **2001**, *42*, 8461−8467.

(2) Guan, L.; Xu, H.; Huang, D. The Investigation on States of Water in Different Hydrophilic Polymers by DSC and FTIR. *J. Polym. Res.* **2011**, *18*, 681−689.

(3) Lee, L. T.; Mann, E. K.; Langevin, D.; Farnoux, B. Neutron Reflectivity and Ellipsometry Studies of a Polymer Molecular Layer Spread on the Water Surface. *Langmuir* **1991**, *7*, 3076−3080.

(4) Kobayashi, M.; Ishihara, K.; Takahara, A. Neutron Reflectivity Study of the Swollen Structure of Polyzwitterion and Polyelectrolyte Brushes in Aqueous Solution. *J. Biomater. Sci. Polym. Ed.* **2014**, *25*, 1673−1686.

(5) Mitamura, K.; Yamada, N. L.; Sagehashi, H.; Torikai, N.; Arita, H.; Terada, M.; Kobayashi, M.; Sato, S.; Seto, H.; Goko, S.; et al. Novel Neutron Reflectometer SOFIA and J-PARC/MLF for in-situ Soft-Interface Characterization. *Polym. J.* **2013**, *45*, 100−108.

(6) Ueda, T.; Murakami, D.; Tanaka, M. Analysis of Interaction Between Interfacial Structure and Fibrinogen at Blood-Compatible Polymer/Water Interface. *Front. Chem.* **2018**, *6*, 542.

(7) Schönherr, H.; Hruska, Z.; Vancso, G. J. Surface Characterization of Oxyfluorinated Isotactic Polypropylene Films: Scanning Force Microscopy with Chemically Modified Probes and Contact Angle Measurements. *Macromolecules* **1998**, *31*, 3679−3685.

(8) Xu, M.; Zhang, C.; Du, Z.; Mi, J. Role of Interfacial Structure of Water in Polymer Surface Wetting. *Macromolecules* **2013**, *46*, 927−934.

(9) Ludwig, R. Water: From Clusters to the Bulk. *Angew. Chem., Int. Ed.* **2001**, *40*, 1808−1827.

(10) Idrissi, A.; Longelin, S.; Sokolić, F. Study of Aqueous Acetone Solution at Various Concentrations: Low-Frequency Raman and Molecular Dynamics Simulations. *J. Phys. Chem. B* **2001**, *105*, 6004−6009.

(11) You, X.; Shirley, J. C.; Lee, E.; Baiz, C. R. Short- and Long-Range Crowding Effects on Water's Hydrogen Bond Networks. *Cell Rep. Phys. Sci.* **2021**, *2*, 100419.

(12) Bakker, H. J.; Skinner, J. L. Vibrational Spectroscopy as a Probe of Structure and Dynamics in Liquid Water. *Chem. Rev.* **2010**, *110*, 1498−1517.

(13) Daly, C. A., Jr.; Streacker, L. M.; Sun, Y.; Pattenaude, S. R.; Hassanali, A. A.; Petersen, P. B.; Corcelli, S. A.; Ben-Amotz, D. Decomposition of the Experimental Raman and Infrared Spectra of Acidic Water into Proton, Special Pair, and Counterion Contributions. *J. Phys. Chem. Lett.* **2017**, *8*, 5246−5252.

(14) Seki, T.; Chiang, K.-Y.; Yu, C.-C.; Yu, X.; Okuno, M.; Hunger, J.; Nagata, Y.; Bonn, M. The Bending Mode of Water: A Powerful Probe for Hydrogen Bond Structure of Aqueous Systems. *J. Phys. Chem. Lett.* **2020**, *11*, 8459−8469.

(15) Kusanagi, H.; Yukawa, S. Fourier Transform Infra-red Spectroscopic Studies of Water Molecules Sorbed in Solid Polymers. *Polymer* **1994**, *35*, 5637−5640.

(16) Sammon, C.; Deng, C.; Yarwood, J. Polymer-Water Interactions. Origin of Perturbed Infrared Intensities of Water in Polymeric Systems. *Polymer* **2003**, *44*, 2669−2677.

(17) Yasoshima, N.; Fukuoka, M.; Kitano, H.; Kagaya, S.; Ishiyama, T.; Gemmei-Ide, M. Diffusion-Controlled Recrystallization of Water

Sorbed into Poly(meth)acrylates Revealed by Variable-Temperature Mid-Infrared Spectroscopy and Molecular Dynamics Simulation. *J. Phys. Chem. B* **2017**, *121*, 5133−5141.
(18) Chen, Z. Investigating Buried Polymer Interfaces using Sum Frequency Generation Vibrational Spectroscopy. *Prog. Polym. Sci.* **2010**, *35*, 1376−1402.
(19) Bülbül, E.; Hegemann, D.; Ataka, K.; Lehner, S.; Heberle, J.; Heuberger, M. Confined Hydration in Nanometer-Graded Plasma Polymer Films: Insights from Surface-Enhanced Infrared Absorption Spectroscopy. *Surf. Interfaces* **2021**, *23*, 100922.
(20) Tanaka, M.; Mochizuki, A. Effect of Water Structure on Blood Compatibility − Thermal Analysis of Water in Poly(meth)acrylate. *J. Biomed. Mater. Res., Part A* **2004**, *68A*, 684−695.
(21) Miwa, Y.; Ishida, H.; Saitô, H.; Tanaka, M.; Mochizuki, A. Network Structures and Dynamics of Dry and Swollen Poly(acrylate)-s. Characterization of High- and Low-Frequency Motions as Revealed by Suppressed or Recovered Intensities (SRI) Analysis of ^{13}C NMR. *Polymer* **2009**, *50*, 6091−6099.
(22) Tanaka, M.; Hayashi, T.; Morita, S. The Roles of Water Molecules at the Biointerface of Medical Polymers. *Polym. J.* **2013**, *45*, 701−710.
(23) Morita, S.; Tanaka, M.; Ozaki, Y. Time-Resolved In Situ ATR-IR Observations of the Process of Sorption of Water into a Poly(2-methoxyethyl acrylate) Film. *Langmuir* **2007**, *23*, 3750−3761.
(24) Kobayashi, S.; Wakui, M.; Iwata, Y.; Tanaka, M. Poly(ω-methoxyalkyl acrylate)s: Nonthrombogenic Polymer Family with Tunable Protein Adsorption. *Biomacromolecules* **2017**, *18*, 4214−4223.
(25) Nishimura, S.; Ueda, T.; Murakami, D.; Tanaka, M. Chain-End Effect for Intermediate Water Formation of Poly(2-Methoxyethyl Acrylate). *Org. Mater.* **2021**, *03*, 214−220.
(26) Ensing, B.; Tiwari, A.; Tros, M.; Hunger, J.; Domingos, S. R.; Pérez, C.; Smits, G.; Bonn, M.; Bonn, D.; Woutersen, S. On the Origin of the Extremely Different Solubilities of Polyethers in Water. *Nat. Commun.* **2019**, *10*, 2893.
(27) Frisch, M. J.; Trucks, G. W.; Schlegel, H. B.; Scuseria, G. E.; Robb, M. A.; Cheeseman, J. R.; Scalmani, G.; Barone, V.; Mennucci, B.; Petersson, G. A.; et al. *Gaussian 09*, revision D.01; Gaussian, Inc.: Wallingford, CT, 2013.
(28) Torii, H.; Ukawa, R. Role of Intermolecular Charge Fluxes in the Hydrogen-Bond-Induced Frequency Shifts of the OH Stretching Mode of Water. *J. Phys. Chem. B* **2021**, *125*, 1468−1475.
(29) Shimanouchi, T. *Tables of Molecular Vibrational Frequencies Consolidated*; National Bureau of Standards: Washington, D.C., 1972; Vol. *I*, pp 1−160.
(30) Schmidt, J. R.; Corcelli, S. A.; Skinner, J. L. Pronounced Non-Condon Effects in the Ultrafast Infrared Spectroscopy of Water. *J. Chem. Phys.* **2005**, *123*, 044513.
(31) Corcelli, S. A.; Skinner, J. L. Infrared and Raman Line Shapes of Dilute HOD in Liquid H_2O and D_2O from 10 to 90 °C. *J. Phys. Chem. A* **2005**, *109*, 6154−6165.
(32) Ohno, K.; Okimura, M.; Akai, N.; Katsumoto, Y. The Effect of Cooperative Hydrogen Bonding on the OH Stretching-Band Shift for Water Clusters Studied by Matrix-Isolation Infrared Spectroscopy and Density Functional Theory. *Phys. Chem. Chem. Phys.* **2005**, *7*, 3005−3014.
(33) Ishii, Y.; Matubayasi, N.; Watanabe, G.; Kato, T.; Washizu, H. Molecular Insights on Confined Water in the Nanochannels of Self-Assembled Ionic Liquid Crystal. *Sci. Adv.* **2021**, *7*, No. eabf0669.

https://doi.org/10.1021/acs.jpcb.2c01702
J. Phys. Chem. B 2022, 126, 4143−4151